catalysts

Article

Efficient Hydrogen Evolution Reaction in 2H-MoS_2 Basal Planes Enhanced by Surface Electron Accumulation

Vimal Krishnamoorthy [1,†], Hemanth Kumar Bangolla [1,†], Chi-Yang Chen [2], Yu-Ting Huang [2], Cheng-Maw Cheng [3,4,5,6], Rajesh Kumar Ulaganathan [7], Raman Sankar [7], Kuei-Yi Lee [2], He-Yun Du [8,9,10,11,*], Li-Chyong Chen [12,13], Kuei-Hsieh Chen [14] and Ruei-San Chen [1,*]

1 Graduate Institute of Applied Science and Technology, National Taiwan University of Science and Technology, Taipei 10607, Taiwan; vimal.cool86@gmail.com (V.K.); hemanthbangolla@gmail.com (H.K.B.)
2 Graduate Institute of Electro-Optical Engineering, National Taiwan University of Science and Technology, Taipei 10607, Taiwan; a0979660804@gmail.com (C.-Y.C.); hyt978@gmail.com (Y.-T.H.); kylee@mail.ntust.edu.tw (K.-Y.L.)
3 National Synchrotron Radiation Research Center, Hsinchu 30076, Taiwan; makalu@nsrrc.org.tw
4 Department of Physics, National Sun Yat-sen University, Kaohsiung 80424, Taiwan
5 Department of Electrophysics, National Yang Ming Chiao Tung University, Hsinchu 300, Taiwan
6 Taiwan Consortium of Emergent Crystalline Materials, National Science and Technology Council, Taipei 10601, Taiwan
7 Institute of Physics, Academia Sinica, Taipei 115201, Taiwan; urajeshiitr@gmail.com (R.K.U.); sankarndf@gmail.com (R.S.)
8 Department of Chemical Engineering, Ming Chi University of Technology, New Taipei City 24301, Taiwan
9 Battery Research Center of Green Energy, Ming Chi University of Technology, New Taipei City 24301, Taiwan
10 Biochemical Engineering Research Center, Ming Chi University of Technology, New Taipei City 24301, Taiwan
11 Center for Sustainability and Energy Technologies, Chang Gung University, Taoyuan City 33302, Taiwan
12 Center for Condensed Matter Sciences, National Taiwan University, Taipei 10617, Taiwan; chenlc@ntu.edu.tw
13 Center of Atomic Initiative for New Materials, National Taiwan University, Taipei 10617, Taiwan
14 Institute of Atomic and Molecular Sciences, Academia Sinica, Taipei 10617, Taiwan
* Correspondence: heyundu@mail.mcut.edu.tw (H.-Y.D.); rsc@mail.ntust.edu.tw (R.-S.C.)
† The authors contributed equally to this work.

Citation: Krishnamoorthy, V.; Bangolla, H.K.; Chen, C.-Y.; Huang, Y.-T.; Cheng, C.-M.; Ulaganathan, R.K.; Sankar, R.; Lee, K.-Y.; Du, H.-Y.; Chen, L.-C.; et al. Efficient Hydrogen Evolution Reaction in 2H-MoS_2 Basal Planes Enhanced by Surface Electron Accumulation. *Catalysts* **2024**, *14*, 50. https://doi.org/10.3390/catal14010050

Academic Editor: Carlo Santoro

Received: 8 December 2023
Revised: 30 December 2023
Accepted: 3 January 2024
Published: 10 January 2024

Abstract: An innovative strategy has been developed to activate the basal planes in molybdenum disulfide (MoS_2) to improve their electrocatalytic activity by controlling surface electron accumulation (SEA) through aging, annealing, and nitrogen-plasma treatments. The optimal hydrogen evolution reaction (HER) performance was obtained on the surface treated with nitrogen-plasma for 120 s. An overpotential of 0.20 V and a Tafel slope of 120 mV dec^{-1} were achieved for the optimized condition. The angle-resolved photoemission spectroscopy measurement confirmed the HER efficiency enhanced by the SEA conjugated with the sulfur vacancy active sites in the MoS_2 basal planes. This study provides new insight into optimizing MoS_2 catalysts for energy applications.

Keywords: molybdenum disulfide; surface electron accumulation; hydrogen evolution reaction; overpotential; Tafel slope

1. Introduction

Hydrogen (H_2) holds great attention as a green energy carrier for future technologies due to its high energy density and being environment friendly [1,2]. Electrochemical water-splitting is a promising route for sustainable H_2 production due to its advantages of abundant sources and non-pollutants [2,3]. Hydrogen evolution reaction (HER) is one of the most efficient pathways to produce H_2 from water splitting using suitable catalysts. Currently, platinum (Pt) and other noble metals or alloys are the most popular electrocatalysts for HER, while their scarcity and high cost limit their widespread utilization [4,5]. The new challenge for researchers is to develop earth-abundant, low-cost, and high-performance catalysts as an alternative to Pt and other noble metals for electrochemical H_2 production.

Two dimensional (2D) transition metal dichalcogenides (TMDCs) have been extensively investigated as promising alternative catalysts for HERs due to their exceptional physicochemical properties including high mechanical properties, good semiconducting ability, large surface area, and high catalytic activity [6–12]. Among TMDCs, molybdenum disulfide (MoS_2) has been found to be one of the most economical alternatives to noble metal catalysts for HER due to its high electron mobility, stability, non-toxic nature, low cost, and excellent electrocatalytic properties [13–15]. Due to its inert basal plane, the overall activity of the two-layered hexagonal phase MoS_2 (2H-phase MoS_2) catalyzes mainly from the active edge sites, which limits the practical application of MoS_2 for HER [9,16–18]. Various techniques have been developed to overcome the limited catalytic activity of the MoS_2 basal plane, such as interface electronic coupling, phase engineering, and introducing active unsaturated defects and strain [19–24]. The pioneer strategy to activate the basal plane of MoS_2 that enhances HER activity was the introduction of sulfur (S)-vacancies into the basal plane [22,25,26].

In HER, the optimal H_2 adsorption free energy (ΔG_H) is 0 eV, where H_2 is bound to the catalyst neither too strongly nor too weakly. For the basal plane of pristine 2H-MoS_2, the ΔG_H value is approximately 2 eV, making the basal plane inert to HER performance. The ΔG_H values can be decreased with an increase in S-vacancies on the MoS_2 basal plane. A ΔG_H value between ± 0.08 eV for S-vacancies in the range of 9–19% is the most favorable value for HER [22,27–29]. To date, a limited number of techniques have been used to create S-vacancies on 2D TMDC materials such as electrochemical reduction, H_2 annealing, and plasma bombardment [29–31]. According to our previous work, long term air exposure (aging) spontaneously creates S-vacancies, which cause surface electron accumulation (SEA) on MoS_2 surfaces [32].

In this report, we utilize and control SEA to activate the basal planes of 2H-MoS_2. The SEA was performed through various techniques such as aging, annealing, and nitrogen (N_2)-plasma treatments to create S-vacancies on the basal plane of 2H-MoS_2. The effect of SEA on HER efficiency was investigated. Angle-resolved photoemission spectroscopy (ARPES) measurements were performed to confirm the electronic structures of different MoS_2 surfaces. The results revealed that 2H-MoS_2 was converted from intrinsic (fresh) to degenerate semiconductor (using N_2-plasma treatments) by creating S-vacancies which provided more active sites and charge carriers for HER.

2. Results and Discussion

2.1. Structural Characterization

Figure 1a illustrates the crystal structure of the MoS_2 monolayer formed by a hexagonal plane of Mo and S atoms. These triple planes are stacked together by weak van der Waals forces of attraction to form bulk MoS_2. The van der Waals force allows the preparation of mono and a few layers of MoS_2 flakes through a simple mechanical exfoliation technique using dicing tape (see Figure 1b). The bulk fresh surface was created by the exfoliation of the top layers of pristine MoS_2 and the other pristine MoS_2 crystal was subjected to N_2-plasma treatments. The X-ray diffraction (XRD) pattern of pristine, fresh, and N_2-plasma-treated bulk samples is shown in Figure 2. The diffraction peaks, located at 14.3°, 29.0°, 44.1°, 60.1°, and 77.9° were assigned to (002), (004), (006), (008), and (0010) planes of standard 2H-MoS_2, respectively (JCPDS #872416) [32]. The diffraction peak along the (002) plane was the most prominent compared with the other peaks. Moreover, a broad reflection around 21° was observed for the fresh and pristine MoS_2 samples which may have been due to the glass substrate [33]. A reduction in the intensity of diffraction peaks of fresh and N_2-plasma MoS_2 was observed when compared with pristine MoS_2, and this may have been due to the absence of constructive interference from the bulk crystal planes [34]. The position of diffraction peaks did not show any shift, which indicated that there was no inner structural change in the MoS_2 samples after N_2-plasma treatment.

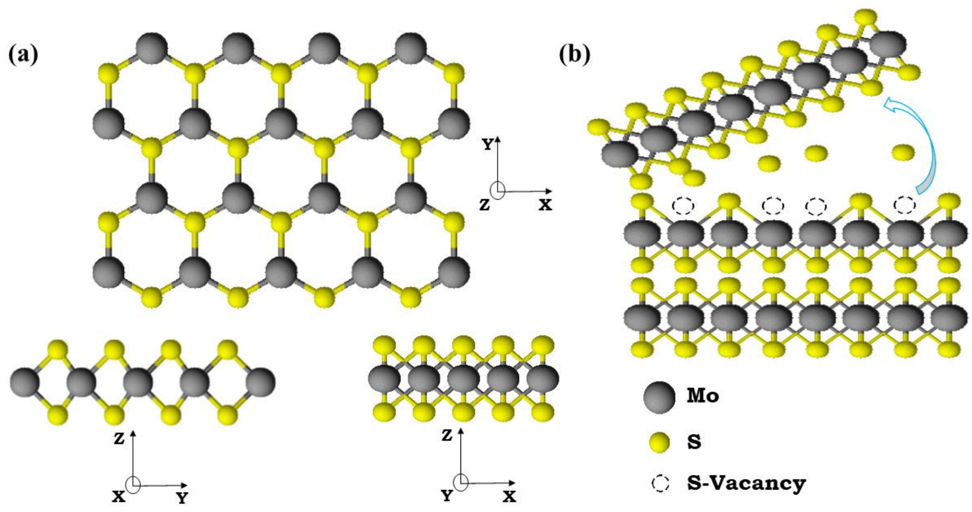

Figure 1. (**a**) The crystal structure of the MoS_2 mono layer. (**b**) The exfoliation process for obtaining a fresh MoS_2 surface and the S-vacancies were created by aging and annealing processes on a fresh surface.

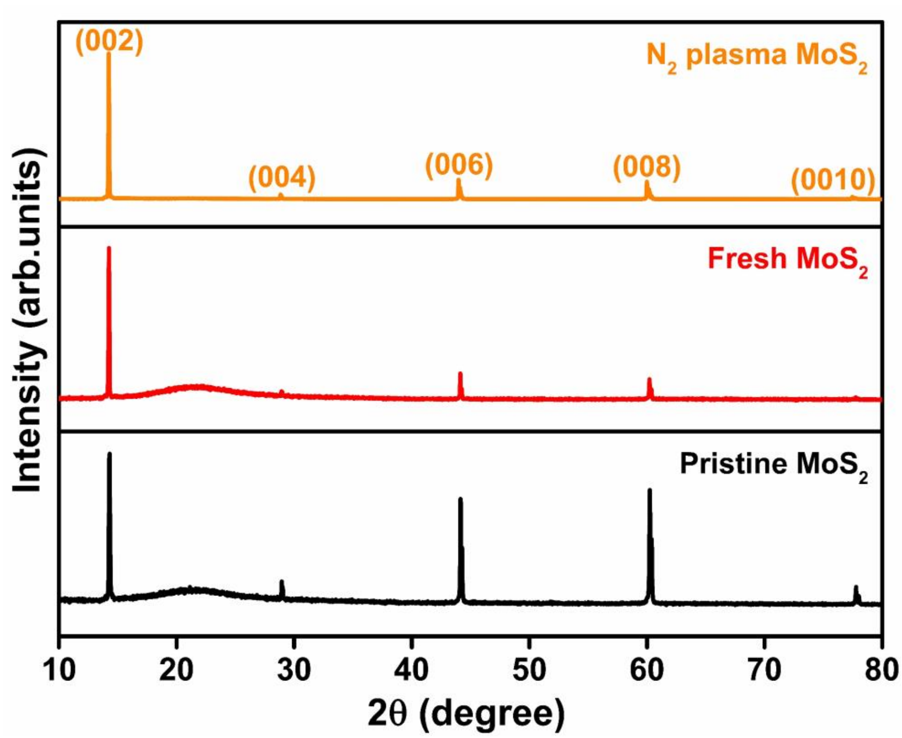

Figure 2. XRD patterns of pristine, fresh, and N_2-plasma-treated MoS_2 bulk.

Figure 3 shows the Raman spectra of pristine, fresh, and N_2-plasma-treated MoS_2. The observed Raman modes at 385 and 411 cm^{-1} belong to the E^1_{2g} (in-plane) and A_{1g} (out-of-plane) modes of bulk MoS_2, respectively [35,36]. The 2H-MoS_2 phase contains four Raman active vibrations, namely, E^1_{2g}, A_{1g}, E_{1g} and E^2_{2g}, and the absence of the other two modes may have been due to the selection rules of the scattering geometry and limited rejection of Rayleigh scattered radiation [35,37,38]. After the exfoliation and plasma treatments, the positions of the observed two modes did not show any shift. However, the peak intensity of the N_2-plasma-treated sample showed considerable decrement when compared with the pristine MoS_2 sample. This indicated that the lattice distortion on the MoS_2 basal plane was due to the gradual increase in S-vacancies and cracks caused by the N_2-plasma treatment [31].

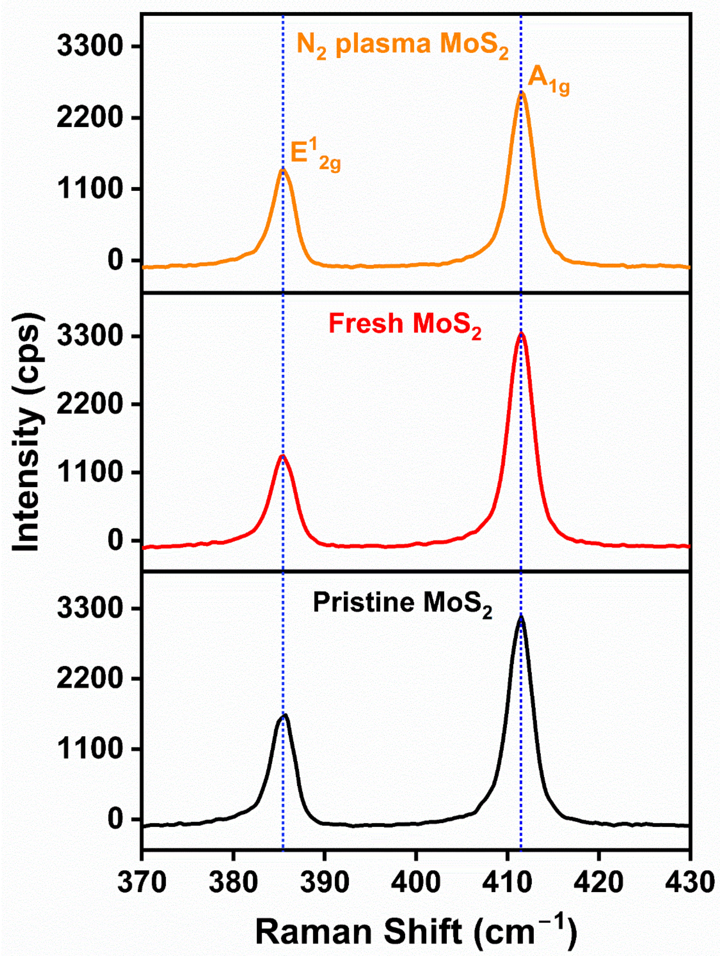

Figure 3. Raman spectra of pristine, fresh, and N_2-plasma-treated MoS_2 bulk.

2.2. Electrochemical HER Efficiency Enhanced by SEA

2.2.1. SEA through Aging

To examine the effects of SEA on a MoS_2 electrocatalyst for a HER, the fresh surface was exposed to air for a different number of days to create SEA on the MoS_2 surface. Figure 4a shows the polarization curves of pristine and fresh MoS_2 surfaces with an overpotential of 0.75 and 0.82 V, respectively. The fresh MoS_2 used a high overpotential of 0.82 V (vs. RHE) to generate a 10 mA/cm^2 current density. The higher overpotential of fresh MoS_2 was due to the intrinsic (insulating) nature of the cleaved fresh surface, which was confirmed by ARPES and scanning tunneling spectroscopy (STS) measurements in our previous study [32]. The overpotential of the fresh surface was reduced by the aging effect, which created the S-vacancies. The aging effect of the fresh surface was examined over a different number of days, and their polarization curves are shown in Figure 4c. The overpotential reduced gradually with the increase in aging time and reached a minimum value of 0.31 V for a surface aging of 58 days. This reduction in the overpotential was evidence of the HER efficiency enhanced by SEA on the MoS_2 basal plane due to the aging effect. Generally, the exposure of the sulfide surface to air causes desulfurization (escape of sulfur atoms) and adsorption of foreign molecules such as oxygen and water molecules. The ARPES results of an in situ-cleaved surface and the same surface kept for 11 h excluded the possibility of the SEA being induced by the adsorption of foreign molecules, and it was concluded that the SEA was induced by long-term air exposure originating from the S-vacancy surface defects [32]. The S-defects created a donor-like surface state close to the conduction band edge which increased the electron concentration at the MoS_2 surface.

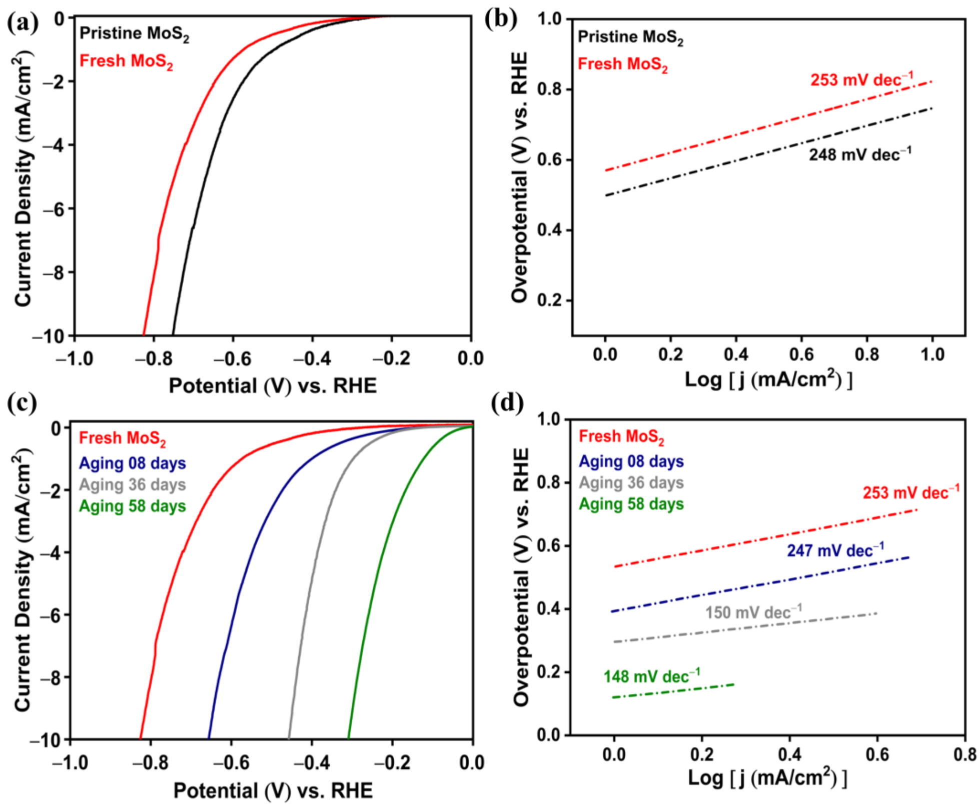

Figure 4. (**a**) Polarization curves and (**b**) corresponding Tafel plots for pristine and fresh surfaces of MoS_2. (**c**) Polarization curves and (**d**) corresponding Tafel plots of fresh and aging surfaces for 8, 36, and 58 days of MoS_2.

Tafel slope is the linear fitting region in the Tafel plot according to the Tafel equation of $\eta = b \log |j| + a$, where η is the overpotential, b is the Tafel slope, and a is the current density [39,40]. The Tafel plots of pristine and fresh MoS_2 surfaces are presented in Figure 4b, with corresponding Tafel slopes of 248 and 253 mV dec^{-1}, respectively. The Tafel plots of aging surfaces are illustrated in Figure 4d, and it was noted that the Tafel slope reduced with an increase in aging time. Finally, the lowest Tafel slope of 148 mV dec^{-1} was obtained for the MoS_2 surface aged for 58 days. Generally, a lower Tafel slope requires less voltage to increase the current density in the HER mechanism by one order of magnitude. Hence, among these, MoS_2 aged for 58 days was the most favorable catalyst for HER. Normally, HER activity depends on the number of active sites on, and electron density of, the catalyst. The major active sites for the electrocatalytic reaction were formed mainly by S-vacancies which were created on the MoS_2 surface due to the spontaneous desulfurization in air [32].

2.2.2. SEA through Annealing

To control the SEA and optimize HER efficiency, the fresh surface was annealed at 80 °C for different times (1, 2, and 3 h). The polarization curves of fresh and annealed MoS_2 surfaces for different times are shown in Figure 5a and corresponding Tafel plots can be seen in Figure 5b. The overpotential of MoS_2 decreased from 0.82 to 0.28 V when the fresh MoS_2 surface was exposed to annealing at 80 °C for 2 h, and the Tafel slope attained the minimum value of 168 mV dec^{-1}. Further, on increasing the heat treatment to 3 h, the overpotential and Tafel slope increased from 0.28 to 0.32 V and 168 to 199 mV dec^{-1}, respectively. This could have been due to the increase in S-vacancies over the optimum when the fresh MoS_2 surface was exposed to heat for more than 2 h. The catalytic activity depends on the density of S-vacancies. Li et al. observed maximal catalytic activity for MoS_2 films when the density of S-vacancies was in the range of 7−10%. Further, an increase in the density of S-vacancies reduced the catalytic activity [41]. Density functional theory studies have revealed that the optimal HER activity of MoS_2 occurs below the S-vacancy concentration of 12.5% [42]. The S-vacancies will disperse homogeneously like point defects up to a vacancy concentration of 12.5%, and with further increases in vacancy concentration (up to 18.75%) some of the vacancies will form agglomerate clusters. At higher vacancy concentrations, the combination of isolated point defects and clustered defects may induce structural defects in MoS_2. The relatively strong hydrogen adsorption ($\Delta G_H = -0.278$ and -0.290 eV) at higher vacancy concentrations (15.63 and 18.75%) shows very high activity for proton adsorption, but desorption of *H to form H_2 would be kinetically more difficult. Hence, the optimal hydrogen adsorption ($\Delta G_H = \pm 0.15$ eV) occurs below the S-vacancy concentration of 12.5%, which corresponds to the highly active sites for hydrogen evolution.

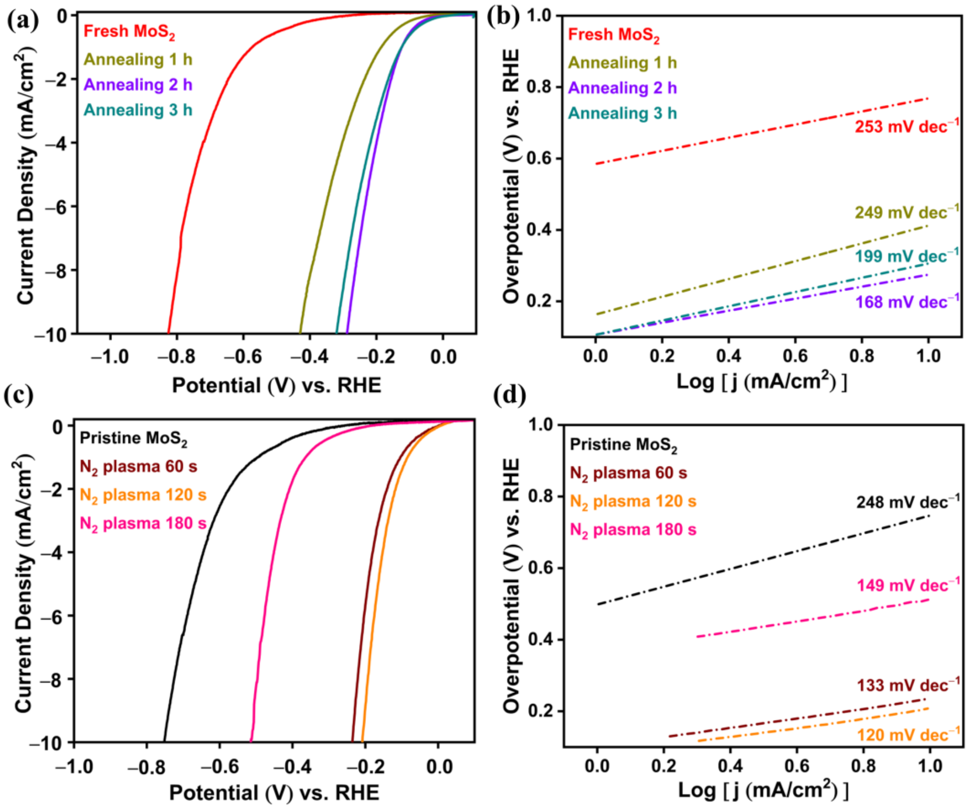

Figure 5. (**a**) Polarization curves and (**b**) corresponding Tafel plots for fresh and annealed MoS_2 at 80 °C for 1, 2, and 3 h. (**c**) Polarization curves and (**d**) corresponding Tafel plots of pristine and N_2-plasma-treated MoS_2 for 60, 120, and 180 s.

2.2.3. SEA through N_2-Plasma Treatment

Further, N_2-plasma treatment was conducted on pristine MoS_2 surfaces over different times to enhance HER activity. The polarization curves and corresponding Tafel plots of pristine and N_2-plasma-treated MoS_2 surfaces over different times are shown in Figures 5c and 5d, respectively. During plasma treatment, the pristine surface was kept 1 cm away from the ICP N_2 plasma generator to avoid rapid S-vacancies and surface damage. The overpotential of the MoS_2 surface reduced from 0.75 to 0.20 V on N_2-plasma exposure for 120 s. Further increases in N_2-plasma exposure time resulted in increases in overpotential. Thus, it was concluded that the optimal N_2-plasma treatment time for better HER activity was 120 s. Generally, the Tafel slopes of 120, 40, and 30 mVdec^{-1} are an indication of the Volmer, Heyrovsky, and Tafel reaction steps in the HER mechanism, respectively [43,44]. The optimal N_2-plasma treatment for 120 s exhibited the Tafel slope value of 120 mV dec^{-1} (see Figure 5d) and hence, it followed the Volmer mechanism of HER.

2.3. Evidence of Enhanced SEA Observed by ARPES

ARPES measurements were performed for the in situ-cleaved, annealed for 2 h, and N_2-plasma treatment for 120 s -MoS_2 surfaces to confirm the existence of SEA as shown in Figure 6a. The magnified normal spectra at Γ point can be seen in Figure 6b. The valence band edge (E_V) of the in situ-cleaved surface was at a binding energy of −0.80 eV which is the indication of intrinsic Fermi level (E_F) according to the bulk MoS_2 band gap of >1.3 eV at 85 K [32]. The difference between E_F and E_V ($E_F - E_V = 0.80$ eV) of the in situ-cleaved surface was in good agreement with the reported value of 0.80 eV for in situ exfoliated MoS_2 under UHV conditions [45]. The SEA of aging surfaces was confirmed by ARPES in our previous work [32]. The E_V of the MoS_2 surface annealed for 2 h resulted in red shift and moved to a binding energy of −1.16 eV. This moved E_F to near the conduction band edge (E_C) ($E_C - E_F = 0.19$ eV). The carrier concentration (n) of the annealing surface can be calculated using the following formula [46]:

$$n = N_C \exp\left[\frac{-(E_C - E_F)}{kT}\right] \quad (1)$$

where N_C is the effective density of states function in the conduction band and is given by $N_C = 2\left(2\pi m_e^* kT/h^2\right)^{\frac{3}{2}}$. Here, m_e^* is the effective mass of an electron, k is Boltzmann's constant, T is the room temperature, and h is Planck's constant. The values of m_e^* for bulk MoS_2 are in the range of 0.45−0.73 m_0; here m_0 is the free electron rest mass [47]. The calculated n of annealing surfaces is 3.4×10^{16}–7.0×10^{16} cm^{-3}.

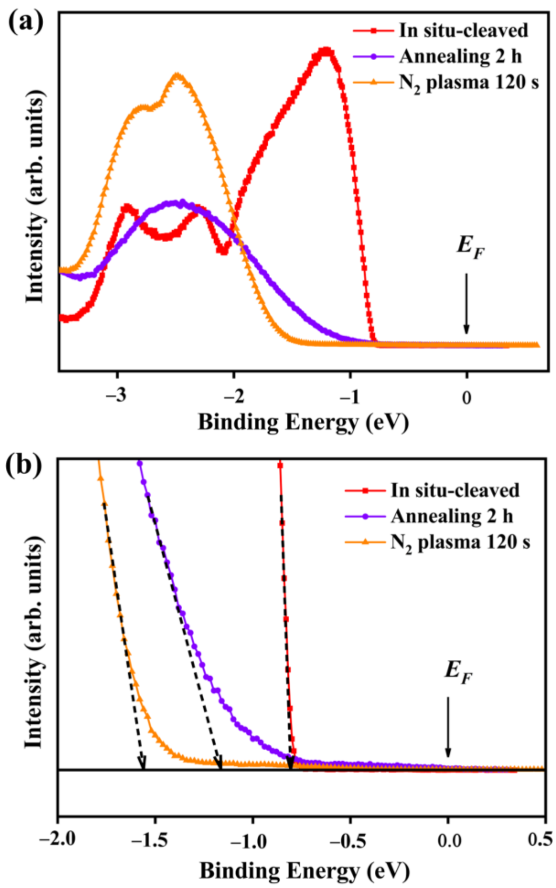

Figure 6. ARPES characterization of MoS_2 surfaces at different conditions. (**a**) The normal emission spectra and (**b**) magnified normal emission spectra of in situ-cleaved, annealed for 2 h, and N_2-plasma-treated for 120 s MoS_2 surfaces. The black dotted lines represent the extrapolation of the linear region of the respective data points to find the E_V values. The experimental data of the in situ-cleaved surface were taken from our previously published work [32].

The E_V showed a remarkable red shift and moved to −1.56 eV for the N_2-plasma-treated MoS_2 surface. This moved the E_F to beyond E_C ($E_F - E_C = 0.26$ eV), which showed the n-type degenerate semiconductor nature. n can be calculated using the following formula [48]:

$$E_F - E_c = kT\left[ln\left(\frac{n}{N_c}\right) + 2^{-3/2}\left(\frac{n}{N_c}\right)\right] \quad (2)$$

The calculated n value was in the range of 1.50×10^{20}–3.10×10^{20} cm^{-3}. This value was around five orders of magnitude higher than the MoS_2 bulk value ($n = 2 \times 10^{15}$ cm^{-3}) [49]. The higher n on the N_2-plasma-treated MoS_2 surface denotes the highly conductive nature of the basal plane. This result was consistent with the electrochemical HER results in which the lowest overpotential was obtained for the N_2-plasma treatment for 120 s on the MoS_2 surface. Hence, it was confirmed that HER activity can be enhanced by producing conjugated active sites and SEA in the 2H-MoS_2 basal plane.

The best HER activity of N_2-plasma-treated MoS_2 with an overpotential of 0.20 V was compared with other MoS_2-based catalysts including nanoflakes [50], thin films [51–53], hierarchical hollow architectures [54], homostructures [55], and hybrid nanostructures [56,57], and is tabulated in Table 1. It was noticed that MoS_2 bulks performed better than MoS_2-based nanostructures and, hence, control of SEA can be a promising strategy to enhance HER activity in 2D TMDCs. In addition, the obtained overpotential of 0.20 V was higher than the overpotential of Ru doped 2H-MoS_2 (0.16 V at 10 $mAcm^{-2}$ in 0.5 M H_2SO_4) [58], and the MoS_2 nanosheet (0.07 V 10 $mAcm^{-2}$ in 0.5 M H_2SO_4 under back-gate voltage of 3V) [59]. This suggests that HER activity in MoS_2 basal planes can be improved further by a combination of SEA with doping or Fermi level modulation.

Table 1. The comparison of MoS_2 bulk overpotential with reported MoS_2 nanostructures.

S. No	System	Overpotential at 10 mA/cm^2 (V)	Reference
1.	MoS_2 bulk (N_2-plasma-treated)	0.20	This work
2.	1T-MoS_2 ultra-thin flakes	0.25	[50]
3.	MoS_2 thin films	0.38	[51]
4.	MoS_2 thin films (ozone treated for 10 min)	0.36	[52]
5.	MoS_2 thin films	0.45	[53]
6.	h-rGO@MoS_2	0.23	[54]
7.	MoS_2 nanosheet/MoS_2 nanoflake	0.26	[55]
8.	MoS_2/GO	0.21	[56]
9.	MoS_2/rGO	0.30	[57]

2.4. Discussion

The schematic of SEA and its enhancement on HER in 2H-MoS_2 is shown in Figure 7. The SEA was produced by the S-vacancies which act as donor-like surface states. The accumulated free electrons were injected from the donor-like surface states and leave the positively charged state on the surface which produced the downward band bending. This moved the E_C below E_F according to the ARPES measurement of the N_2-plasma-treated MoS_2 surface due to its n-type degenerate nature. S-vacancies are the origin of high surface electron concentration and, meanwhile, provide abundant active sites. The conjugated SEA and HER active sites provide the required conditions to enhance the electrochemical activity of HER.

Usually, in MoS_2, the metallic 1T-phase basal plane is considered for the HER due to the possible source of active sites [9,23]. The SEA in 2H-MoS_2 enhances HER activity and this result may be comparable with the excellent HER activity of the metallic 1T-phase MoS_2 [7,23,60]. In our previous reports, we observed SEA formation in MoS_2 and $MoSe_2$ due to the S- and Se-vacancies, respectively [32,48]. The MoS_2 catalyst has been widely investigated for HER but, unexpectedly, the effect of SEA on HER efficiency has been ignored in previous reports. This investigation gives a new insight into the tuning of basal plane active sites through S-vacancies by keeping the edge defects that can enhance HER activity. Moreover, the catalytic vacancy sites and abundant free electrons at the surface are the major areas responsible for efficient HER activity.

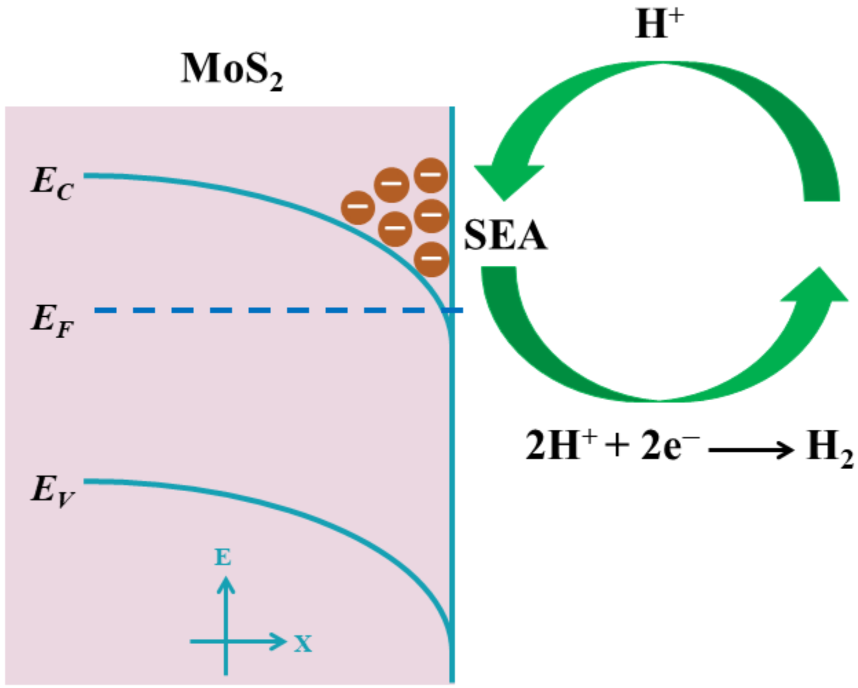

Figure 7. Schematic diagram of SEA and its effect on HER in MoS_2. Surface band bending and SEA are produced by the donor-like surface states.

3. Experimental Section

3.1. Preparation of MoS_2 Layer Crystals

The chemical vapor transport method was used to synthesize MoS_2 single crystals. Fine powders of sulfur (99.99%) and molybdenum (99.99%) were used as source materials. Bromine (Br_2) was used as the transport agent and enabled an effective and faster vapor transport to produce MoS_2 single crystals. The source materials including sulfur and molybdenum powders together with Br_2 were sealed in a quartz ampoule of a length of 30 cm at a vacuum of 10^{-5} Torr. The inner and outer diameters of the quartz ampoule were 1.3 and 1.6 cm, respectively. The preheated material temperatures of growth MoS_2 single crystals were kept at 950 and 1000 °C, respectively. The controlling temperatures of the source and crystallization ends were maintained at 1050 and 960 °C, respectively. After ten days of processing, the as-synthesized MoS_2 layer crystals area was in the range of a few square millimeters to centimeters. The thickness of the crystals ranged from a few nanometers to hundreds of nanometers. Typical mechanical exfoliation was used for obtaining fresh surface MoS_2 from the pristine layer crystals using dicing tape.

3.2. Characterization of MoS_2 Bulks

An X-ray diffraction (XRD-Bruker D_2 phaser diffractometer) system with Cu $K_{\alpha 1}$ radiation (λ = 1.54056 Å) and Raman spectroscopy (Jobin-Yvon LabRAM HR800) with a 633 nm He-Ne laser as the excitation source were used to examine the structural characterization of the MoS_2 bulks. The pristine surface (non-fresh) meant that the surface of the as-synthesized crystal was exposed to air for a prolonged period. The fresh surface was obtained by stripping the top layers of the bulk crystal with dicing tape. The N_2-plasma treatment was performed on a different pristine MoS_2 surface.

3.3. N_2-Plasma Treatment of Pristine MoS_2

An inductively coupled plasma (ICP) system with a commercial 13.56 MHz RF source was used to perform the N_2-plasma treatment on the MoS_2/glassy carbon electrode. In the quartz tube, the distance between the samples and the center of the coil was maintained at 1 cm and the samples were placed on the downstream side. After that, the vacuum in the chamber was maintained at 10 mTorr. High purity N_2 (99.999%) was allowed into the quartz tube at a flow rate of 400 sccm. The N_2-plasma was generated under a pressure of 130 mTorr due to excited N_2 ions when powered by 100 W at ambient temperature. Finally, the pristine MoS_2 surfaces were exposed to a N_2-plasma atmosphere for fixed different time intervals.

3.4. Electrochemical Measurements

An electrochemical test system (Biologic Bi-stat) was used to perform the HER activity measurements using a standard three electrode cell at ambient temperature. The working electrode had a rotating disk electrode (RDE, PINE AFE5T050GC) with a glassy carbon (GC) disk (diameter 5 mm) and a PTFE shroud (diameter 15 mm). The platinum foil and Ag/AgCl were utilized as counter and reference electrodes, respectively. The measured potential values were transferred to a reversible hydrogen electrode (RHE), where $E_{RHE} = E_{Ag/AgCl} + 0.059\ pH + E^{\circ}{}_{Ag/AgCl}$. The HER polarization curves were recorded in a 0.5 M H_2SO_4 (pH $\approx$ 0.3) electrolyte at a scan rate of 5 mVs^{-1}. The high purity N_2 gas was passed through the electrolyte to remove other gases. As-prepared MoS_2 catalyst was loaded onto the surface of the GC electrode and thread sealant (Loctite®) was used to cover the uncovered GC area beside the MoS_2 catalyst. For the pristine surface, the bulk MoS_2 crystal was placed on the surface of the GC electrode and fixed. For the fresh surface, first we fixed the pristine bulk on the GC electrode and removed the top surface using dicing tape; then for the annealing process, the electrode with the fresh surface was exposed to heating. For the N_2-plasma-treated samples, first we fixed the pristine bulk on the GC electrode and then exposed it to plasma. Cyclic voltammetry (CV) was performed in the potential range of -1.0 to +0.2 V (vs. RHE) and a scan rate of 50 mVs^{-1} until the curves reached a stable state. Linear sweep voltammetry (LSV) was executed in the same potential range as CV with a scan rate of 5 mVs^{-1}. The electrochemical measurements were repeated three times to obtain concordant data.

3.5. Angle-Resolved Photoelectron Spectroscopy (ARPES) Measurement

The ARPES experiment was performed at the National Synchrotron Radiation Research Center (NSRRC) in Hsinchu, Taiwan, at a BL21B1 U9-CGM beamline. The photoemission spectra of MoS_2 annealed and N_2-plasma-treated surfaces were measured in a UHV chamber equipped with a hemispherical analyzer (Scienta R4000) with a collecting angle of $\pm 15^{\circ}$ at a base pressure of 5.6×10^{-11} Torr. The polarization was invariably in the angular dispersive plane. The spectra of all MoS_2 surfaces were recorded with a photon energy of 42 eV at 85 K. The energy resolution was better than 23 meV and the angular resolution was 0.2°. After loading samples into a load–lock vacuum chamber, the samples were left in a vacuum until the pressure and temperature reached the required steady state.

4. Conclusions

We improved the electrocatalytic activity of 2H-MoS_2 by activating its basal planes through SEA using aging, annealing, and nitrogen-plasma treatments. The SEA caused by the S-vacancies was catalytically active, and a high electron concentration in the order of ~10^{20} cm^{-3} was obtained for the N_2-plasma-treated MoS_2 surface. The optimal HER performance was obtained for the surface which underwent N_2-plasma treatment for 120 s, with an overpotential of 0.20 V vs RHE at 10 mA cm^{-2}. The ARPES measurements confirmed that the HER efficiency enhanced by the SEA conjugated with the S-vacancy active sites in the 2H-MoS_2 basal planes. This work provides an efficient and low cost MoS_2-based HER catalyst and also opens up comprehensive insights into basal planes of 2D TMDCs through SEA for energy related applications.

Author Contributions: Conceptualization and writing—review and editing, R.-S.C.; methodology, V.K., C.-Y.C., Y.-T.H. and C.-M.C.; formal analysis and writing—original draft preparation, V.K. and H.K.B.; investigation, C.-M.C., R.K.U., R.S., K.-Y.L., H.-Y.D. and L.-C.C.; supervision, H.-Y.D., L.-C.C., K.-H.C. and R.-S.C.; resources and validation, L.-C.C., K.-H.C. and R.-S.C. All authors have read and agreed to the published version of the manuscript.

Funding: This research was funded by Ministry of Science and Technology (MOST) of Taiwan grant numbers MOST 111-2112-M-011-004-MY3, MOST 108-2628-M-011-001-MY3, MOST 109-2622-E-011-034, MOST 110-2622-E-011-017, MOST 112-2112-M-131-003, MOST 111-2112-M-131-003, NSTC 112-2124-M-001-007 and NSTC 112-2811-M-001-065, Chang Gung University, Taiwan grant number URRPD2N0021, and the Academia Sinica, Taiwan grant number AS-iMATE-112-12. And the APC was funded by Ministry of Science and Technology (MOST) of Taiwan.

Data Availability Statement: The data presented in this study are available on request from the corresponding author.

Acknowledgments: Corresponding author R.-S.C. thanks the support of the Ministry of Science and Technology (MOST) of Taiwan. Corresponding author H.-Y.D. expresses gratitude for the financial support provided by Ministry of Science and Technology (MOST) of Taiwan and Chang Gung University, Taiwan. Author R.S. acknowledges the financial support provided by the Ministry of Science and Technology (MOST) of Taiwan and Academia Sinica, Taiwan. Author V.K. thanks the Ministry of Education (MOE) Elite Scholarship Program and the National Taiwan University of Science and Technology (NTUST) Scholarship Program for additional financial support.

Conflicts of Interest: The authors declare no conflicts of interest.

References

1. Shi, Y.; Zhou, Y.; Yang, D.R.; Xu, W.X.; Wang, C.; Wang, F.B.; Xu, J.J.; Xia, X.H.; Chen, H.Y. Energy Level Engineering of MoS_2 by Transition-Metal Doping for Accelerating Hydrogen Evolution Reaction. *J. Am. Chem. Soc.* **2017**, *139*, 15479–15485. [CrossRef]
2. Wang, J.; Yan, M.; Zhao, K.; Liao, X.; Wang, P.; Pan, X.; Yang, W.; Mai, L. Field Effect Enhanced Hydrogen Evolution Reaction of MoS_2 Nanosheets. *Adv. Mater.* **2017**, *29*, 1604464. [CrossRef]
3. Tachibana, Y.; Vayssieres, L.; Durrant, J.R. Artificial Photosynthesis for Solar Water-Splitting. *Nat. Photonics* **2012**, *6*, 511–518. [CrossRef]
4. Ouyang, Y.; Ling, C.; Chen, Q.; Wang, Z.; Shi, L.; Wang, J. Activating Inert Basal Planes of MoS_2 for Hydrogen Evolution Reaction through the Formation of Different Intrinsic Defects. *Chem. Mater.* **2016**, *28*, 4390–4396. [CrossRef]
5. Ding, Q.; Song, B.; Xu, P.; Jin, S. Efficient Electrocatalytic and Photoelectrochemical Hydrogen Generation Using MoS_2 and Related Compounds. *Chem* **2016**, *1*, 699–726. [CrossRef]
6. Prabhu, P.; Jose, V.; Lee, J.M. Design Strategies for Development of TMD-Based Heterostructures in Electrochemical Energy Systems. *Matter* **2020**, *2*, 526–553. [CrossRef]
7. Ambrosi, A.; Sofer, Z.; Pumera, M. 2H → 1T Phase Transition and Hydrogen Evolution Activity of MoS_2, $MoSe_2$, WS_2 and WSe_2 Strongly Depends on the MX_2 Composition. *Chem. Commun.* **2015**, *51*, 8450–8453. [CrossRef] [PubMed]
8. Zhu, C.; Gao, D.; Ding, J.; Chao, D.; Wang, J. TMD-Based Highly Efficient Electrocatalysts Developed by Combined Computational and Experimental Approaches. *Chem. Soc. Rev.* **2018**, *47*, 4332–4356. [CrossRef] [PubMed]
9. Voiry, D.; Salehi, M.; Silva, R.; Fujita, T.; Chen, M.; Asefa, T.; Shenoy, V.B.; Eda, G.; Chhowalla, M. Conducting MoS_2 Nanosheets as Catalysts for Hydrogen Evolution Reaction. *Nano Lett.* **2013**, *13*, 6222–6227. [CrossRef]
10. Lukowski, M.A.; Daniel, A.S.; English, C.R.; Meng, F.; Forticaux, A.; Hamers, R.J.; Jin, S. Highly Active Hydrogen Evolution Catalysis from Metallic WS_2 Nanosheets. *Energy Environ. Sci.* **2014**, *7*, 2608–2613. [CrossRef]
11. Mahler, B.; Hoepfner, V.; Liao, K.; Ozin, G.A. Colloidal Synthesis of 1T-WS_2 and 2H-WS_2 Nanosheets: Applications for Photocatalytic Hydrogen Evolution. *J. Am. Chem. Soc.* **2014**, *136*, 14121–14127. [CrossRef] [PubMed]
12. Lazar, P.; Otyepka, M. Role of the Edge Properties in the Hydrogen Evolution Reaction on MoS_2. *Chem. Eur. J.* **2017**, *23*, 4863–4869. [CrossRef] [PubMed]
13. Cao, Y. Roadmap and Direction toward High-Performance MoS_2 Hydrogen Evolution Catalysts. *ACS Nano* **2021**, *15*, 11014–11039. [CrossRef] [PubMed]
14. Wu, Z.; Fang, B.; Wang, Z.; Wang, C.; Liu, Z.; Liu, F.; Wang, W.; Alfantazi, A.; Wang, D.; Wilkinson, D.P. MoS_2 Nanosheets: A Designed Structure with High Active Site Density for the Hydrogen Evolution Reaction. *ACS Catal.* **2013**, *3*, 2101–2107. [CrossRef]
15. Wu, L.; Longo, A.; Dzade, N.Y.; Sharma, A.; Hendrix, M.M.R.M.; Bol, A.A.; de Leeuw, N.H.; Hensen, E.J.M.; Hofmann, J.P. The Origin of High Activity of Amorphous MoS_2 in the Hydrogen Evolution Reaction. *ChemSusChem* **2019**, *12*, 4383–4389. [CrossRef] [PubMed]
16. Wang, Y.; Carey, B.J.; Zhang, W.; Chrimes, A.F.; Chen, L.; Kalantar-Zadeh, K.; Ou, J.Z.; Daeneke, T. Intercalated 2D MoS_2 Utilizing a Simulated Sun Assisted Process: Reducing the HER Overpotential. *J. Phys. Chem. C* **2016**, *120*, 2447–2455. [CrossRef]

17. Er, D.; Ye, H.; Frey, N.C.; Kumar, H.; Lou, J.; Shenoy, V.B. Prediction of Enhanced Catalytic Activity for Hydrogen Evolution Reaction in Janus Transition Metal Dichalcogenides. *Nano Lett.* **2018**, *18*, 3943–3949. [CrossRef] [PubMed]
18. Ye, G.; Gong, Y.; Lin, J.; Li, B.; He, Y.; Pantelides, S.T.; Zhou, W.; Vajtai, R.; Ajayan, P.M. Defects Engineered Monolayer MoS_2 for Improved Hydrogen Evolution Reaction. *Nano Lett.* **2016**, *16*, 1097–1103. [CrossRef]
19. Voiry, D.; Fullon, R.; Yang, J.; DeCarvalho Castro E Silva, C.; Kappera, R.; Bozkurt, I.; Kaplan, D.; Lagos, M.J.; Batson, P.E.; Gupta, G.; et al. The Role of Electronic Coupling between Substrate and 2D MoS_2 Nanosheets in Electrocatalytic Production of Hydrogen. *Nat. Mater.* **2016**, *15*, 1003–1009. [CrossRef]
20. Zhu, J.; Wang, Z.C.; Dai, H.; Wang, Q.; Yang, R.; Yu, H.; Liao, M.; Zhang, J.; Chen, W.; Wei, Z.; et al. Boundary Activated Hydrogen Evolution Reaction on Monolayer MoS_2. *Nat. Commun.* **2019**, *10*, 1348. [CrossRef] [PubMed]
21. Yin, Y.; Han, J.; Zhang, Y.; Zhang, X.; Xu, P.; Yuan, Q.; Samad, L.; Wang, X.; Wang, Y.; Zhang, Z.; et al. Contributions of Phase, Sulfur Vacancies, and Edges to the Hydrogen Evolution Reaction Catalytic Activity of Porous Molybdenum Disulfide Nanosheets. *J. Am. Chem. Soc.* **2016**, *138*, 7965–7972. [CrossRef] [PubMed]
22. Li, H.; Tsai, C.; Koh, A.L.; Cai, L.; Contryman, A.W.; Fragapane, A.H.; Zhao, J.; Han, H.S.; Manoharan, H.C.; Abild-Pedersen, F.; et al. Erratum: Activating and Optimizing MoS_2 Basal Planes for Hydrogen Evolution through the Formation of Strained Sulphur Vacancies. *Nat. Mater.* **2016**, *15*, 364. [CrossRef] [PubMed]
23. Lukowski, M.A.; Daniel, A.S.; Meng, F.; Forticaux, A.; Li, L.; Jin, S. Enhanced Hydrogen Evolution Catalysis from Chemically Exfoliated Metallic MoS_2 Nanosheets. *J. Am. Chem. Soc.* **2013**, *135*, 10274–10277. [CrossRef] [PubMed]
24. Bolar, S.; Shit, S.; Murmu, N.C.; Samanta, P.; Kuila, T. Activation Strategy of MoS_2 as HER Electrocatalyst through Doping-Induced Lattice Strain, Band Gap Engineering, and Active Crystal Plane Design. *ACS Appl. Mater. Interfaces* **2021**, *13*, 765–780. [CrossRef] [PubMed]
25. Lu, A.Y.; Yang, X.; Tseng, C.C.; Min, S.; Lin, S.H.; Hsu, C.L.; Li, H.; Idriss, H.; Kuo, J.L.; Huang, K.W.; et al. High-Sulfur-Vacancy Amorphous Molybdenum Sulfide as a High Current Electrocatalyst in Hydrogen Evolution. *Small* **2016**, *12*, 5530–5537. [CrossRef] [PubMed]
26. Li, H.; Du, M.; Mleczko, M.J.; Koh, A.L.; Nishi, Y.; Pop, E.; Bard, A.J.; Zheng, X. Kinetic Study of Hydrogen Evolution Reaction over Strained MoS_2 with Sulfur Vacancies Using Scanning Electrochemical Microscopy. *J. Am. Chem. Soc.* **2016**, *138*, 5123–5129. [CrossRef] [PubMed]
27. Hinnemann, B.; Moses, P.G.; Bonde, J.; Jørgensen, K.P.; Nielsen, J.H.; Horch, S.; Chorkendorff, I.; Nørskov, J.K. Biomimetic Hydrogen Evolution: MoS_2 Nanoparticles as Catalyst for Hydrogen Evolution. *J. Am. Chem. Soc.* **2005**, *127*, 5308–5309. [CrossRef]
28. Tsai, C.; Chan, K.; Nørskov, J.K.; Abild-Pedersen, F. Theoretical Insights into the Hydrogen Evolution Activity of Layered Transition Metal Dichalcogenides. *Surf. Sci.* **2015**, *640*, 133–140. [CrossRef]
29. Tsai, C.; Abild-Pedersen, F.; Nørskov, J.K. Tuning the MoS_2 Edge-Site Activity for Hydrogen Evolution via Support Interactions. *Nano Lett.* **2014**, *14*, 1381–1387. [CrossRef]
30. Kiriya, D.; Lobaccaro, P.; Nyein, H.Y.Y.; Taheri, P.; Hettick, M.; Shiraki, H.; Sutter-Fella, C.M.; Zhao, P.; Gao, W.; Maboudian, R.; et al. General Thermal Texturization Process of MoS_2 for Efficient Electrocatalytic Hydrogen Evolution Reaction. *Nano Lett.* **2016**, *16*, 4047–4053. [CrossRef]
31. Nguyen, A.D.; Nguyen, T.K.; Le, C.T.; Kim, S.; Ullah, F.; Lee, Y.; Lee, S.; Kim, K.; Lee, D.; Park, S.; et al. Nitrogen-Plasma-Treated Continuous Monolayer MoS_2 for Improving Hydrogen Evolution Reaction. *ACS Omega* **2019**, *4*, 21509–21515. [CrossRef] [PubMed]
32. Siao, M.D.; Shen, W.C.; Chen, R.S.; Chang, Z.W.; Shih, M.C.; Chiu, Y.P.; Cheng, C.M. Two-Dimensional Electronic Transport and Surface Electron Accumulation in MoS_2. *Nat. Commun.* **2018**, *9*, 1442. [CrossRef] [PubMed]
33. Mikhalitsyna, E.A.; Kataev, V.A.; Larrañaga, A.; Lepalovskij, V.N.; Kurlyandskaya, G.V. Nanocrystallization in FINEMET-Type $Fe_{73.5}Nb_3Cu_1Si_{13.5}B_9$ and $Fe_{72.5}Nb_{1.5}Mo_2Cu_{1.1}Si_{14.2}B_{8.7}$ Thin Films. *Materials* **2020**, *13*, 348. [CrossRef] [PubMed]
34. Sahoo, D.; Kumar, B.; Sinha, J.; Ghosh, S.; Roy, S.S.; Kaviraj, B. Cost Effective Liquid Phase Exfoliation of MoS_2 Nanosheets and Photocatalytic Activity for Wastewater Treatment Enforced by Visible Light. *Sci. Rep.* **2020**, *10*, 10759. [CrossRef] [PubMed]
35. Li, H.; Zhang, Q.; Yap, C.C.R.; Tay, B.K.; Edwin, T.H.T.; Olivier, A.; Baillargeat, D. From Bulk to Monolayer MoS_2: Evolution of Raman Scattering. *Adv. Funct. Mater.* **2012**, *22*, 1385–1390. [CrossRef]
36. Molina-Sánchez, A.; Hummer, K.; Wirtz, L. Vibrational and Optical Properties of MoS_2: From Monolayer to Bulk. *Surf. Sci. Rep.* **2015**, *70*, 554–586. [CrossRef]
37. Verble, J.L.; Wieting, T.J. Lattice Mode Degeneracy in MoS_2 and Other Layer Compounds. *Phys. Rev. Lett.* **1970**, *25*, 362–365. [CrossRef]
38. Kong, D.; Wang, H.; Cha, J.J.; Pasta, M.; Koski, K.J.; Yao, J.; Cui, Y. Synthesis of MoS_2 and $MoSe_2$ Films with Vertically Aligned Layers. *Nano Lett.* **2013**, *13*, 1341. [CrossRef]
39. Sarker, S.; Peters, J.; Chen, X.; Li, B.; Chen, G.; Yan, L.; Richins, S.K.; Das, S.; Zhou, M.; Luo, H. Engineering Molybdenum Diselenide and Its Reduced Graphene Oxide Hybrids for Efficient Electrocatalytic Hydrogen Evolution. *ACS Appl. Nano Mater.* **2018**, *1*, 2143–2152. [CrossRef]
40. Zhang, L.; Wang, T.; Sun, L.; Sun, Y.; Hu, T.; Xu, K.; Ma, F. Hydrothermal Synthesis of 3D Hierarchical $MoSe_2/NiSe_2$ Composite Nanowires on Carbon Fiber Paper and Their Enhanced Electrocatalytic Activity for the Hydrogen Evolution Reaction. *J. Mater. Chem. A* **2017**, *5*, 19752–19759. [CrossRef]

41. Li, G.; Zhang, D.; Qiao, Q.; Yu, Y.; Peterson, D.; Zafar, A.; Kumar, R.; Curtarolo, S.; Hunte, F.; Shannon, S.; et al. All The Catalytic Active Sites of MoS_2 for Hydrogen Evolution. *J. Am. Chem. Soc.* **2016**, *138*, 16632–16638. [CrossRef] [PubMed]
42. Zhou, W.; Dong, L.; Tan, L.; Tang, Q. First-Principles Study of Sulfur Vacancy Concentration Effect on the Electronic Structures and Hydrogen Evolution Reaction of MoS_2. *Nanotechnology* **2021**, *32*, 145718. [CrossRef] [PubMed]
43. Li, S.; Wang, S.; Salamone, M.M.; Robertson, A.W.; Nayak, S.; Kim, H.; Tsang, S.C.E.; Pasta, M.; Warner, J.H. Edge-Enriched 2D MoS_2 Thin Films Grown by Chemical Vapor Deposition for Enhanced Catalytic Performance. *ACS Catal.* **2017**, *7*, 877–886. [CrossRef]
44. Sun, Y.; Alimohammadi, F.; Zhang, D.; Guo, G. Enabling Colloidal Synthesis of Edge-Oriented MoS_2 with Expanded Interlayer Spacing for Enhanced HER Catalysis. *Nano Lett.* **2017**, *17*, 1963–1969. [CrossRef]
45. Wang, X.; Cormier, C.R.; Khosravi, A.; Smyth, C.M.; Shallenberger, J.R.; Addou, R.; Wallace, R.M. In Situ Exfoliated 2D Molybdenum Disulfide Analyzed by XPS. *Surf. Sci. Spectra* **2020**, *27*, 014019. [CrossRef]
46. Neamen, D.A. *Semiconductor Physics and Devices: Basic Principles*, 4th ed.; McGraw Hill: New York, NY, USA, 2012.
47. Peelaers, H.; Van DeWalle, C.G. Effects of Strain on Band Structure and Effective Masses in MoS_2. *Phys. Rev. B* **2012**, *86*, 241401. [CrossRef]
48. Chang, Y.S.; Chen, C.Y.; Ho, C.J.; Cheng, C.M.; Chen, H.R.; Fu, T.Y.; Huang, Y.T.; Ke, S.W.; Du, H.Y.; Lee, K.Y.; et al. Surface Electron Accumulation and Enhanced Hydrogen Evolution Reaction in $MoSe_2$ Basal Planes. *Nano Energy* **2021**, *84*, 105922. [CrossRef]
49. Tiong, K.K.; Liao, P.C.; Ho, C.H.; Huang, Y.S. Growth and Characterization of Rhenium-Doped MoS Single Crystals. *J. Cryst. Growth* **1999**, *205*, 543–547. [CrossRef]
50. Yang, F.; Cao, Z.-F.; Wang, J.; Wang, S.; Zhong, H. Novel Preparation of High Activity 1T-Phase MoS_2 Ultra-Thin Flakes by Layered Double Hydroxide for Enhanced Hydrogen Evolution Performance. *Int. J. Hydrog. Energy* **2019**, *44*, 21229–21237. [CrossRef]
51. Kim, J.; Takahashi, K.; Takaetsu, T.; Funatsu, T. Characterization of Vertically Aligned MoS_2 Thin Film on Mo Electrode for Hydrogen Evolution Catalyst. *J. Jpn. Inst. Energy* **2021**, *100*, 283–287. [CrossRef]
52. Bhimanapati, G.R.; Hankins, T.; Lei, Y.; Vilá, R.A.; Fuller, I.; Terrones, M.; Robinson, J.A. Growth and Tunable Surface Wettability of Vertical MoS_2 Layers for Improved Hydrogen Evolution Reactions. *ACS Appl. Mater. Interfaces* **2016**, *8*, 22190–22195. [CrossRef]
53. Liu, N.; Kim, J.; Oh, J.; Nguyen, Q.T.; Sahu, B.B.; Han, J.G.; Kim, S. Growth of Multiorientated Polycrystalline MoS_2 Using Plasma-Enhanced Chemical Vapor Deposition for Efficient Hydrogen Evolution Reactions. *Nanomaterials* **2020**, *10*, 1465. [CrossRef] [PubMed]
54. Zheng, S.; Zheng, L.; Zhu, Z.; Chen, J.; Kang, J.; Huang, Z.; Yang, D. MoS_2 Nanosheet Arrays Rooted on Hollow RGO Spheres as Bifunctional Hydrogen Evolution Catalyst and Supercapacitor Electrode. *Nano-Micro Lett.* **2018**, *10*, 62. [CrossRef] [PubMed]
55. Yang, L.; Zhang, J.; Feng, C.; Xu, G.; Xie, C.; Yuan, X.; Xiang, B. MoS_2 Nanosheet/MoS_2 Flake Homostructures for Efficient Electrocatalytic Hydrogen Evolution MoS_2 Nanosheet/MoS_2 Fl Ake Homostructures for Efficient Electrocatalytic Hydrogen Evolution. *Mater. Res. Express* **2019**, *6*, 085005. [CrossRef]
56. Bojarska, Z.; Mazurkiewicz-Pawlicka, M.; Mierzwa, B.; Plocinski, T.; Makowski, L. Effect of the Carbon Support on MoS_2 hybrid Nanostructures Prepared by an Impinging Jet Reactor for Hydrogen Evolution Reaction Catalysis. *J. Environ. Chem. Eng.* **2022**, *10*, 108038. [CrossRef]
57. Singh, A.K.; Prasad, J.; Azad, U.P.; Singh, A.K.; Prakash, R.; Singh, K.; Srivastava, A.; Alaferdov, A.A.; Moshkalev, S.A. Vanadium Doped Few-Layer Ultrathin MoS_2 Nanosheets on Reduced Graphene Oxide for High-Performance Hydrogen Evolution Reaction. *RSC Adv.* **2019**, *9*, 22232–22239. [CrossRef] [PubMed]
58. Wang, J.; Fang, W.; Hu, Y.; Zhang, Y.; Dang, J.; Wu, Y.; Chen, B.; Zhao, H.; Li, Z. Single Atom Ru Doping 2H-MoS_2 as Highly Efficient Hydrogen Evolution Reaction Electrocatalyst in a Wide pH Range. *Appl. Catal. B Environ.* **2021**, *298*, 120490. [CrossRef]
59. Zhang, W.; Liao, X.; Pan, X.; Yan, M.; Li, Y.; Tian, X.; Zhao, Y.; Xu, L.; Mai, L. Superior Hydrogen Evolution Reaction Performance in 2H-MoS_2 to That of 1T Phase. *Small* **2019**, *15*, 1900964. [CrossRef]
60. Tang, Q.; Jiang, D.E. Mechanism of Hydrogen Evolution Reaction on 1T-MoS_2 from First Principles. *ACS Catal.* **2016**, *6*, 4953–4961. [CrossRef]